J. Phys. D: Appl. Phys. **33** (2000) 430–436. Printed in the UK PII: S0022-3727(00)03964-4

Thermal and acoustic pulse studies of space-charge profiles in electron-irradiated fluoroethylene propylene

P Bloß†‖, A S DeReggi†, G-M Yang‡, G M Sessler‡¶ and H Schäfer§

† Polymers Division, Building 224/Room B320, National Institute of Standards and Technology, Gaithersburg, MD 20899, USA
‡ Institute for Telecommunication and Electroacoustics, Technical University Darmstadt, Merckstr. 25, D-64283 Darmstadt, Germany
§ HF-NMR Facility, NSR Center, University of Nijmegen, Toernooiveld 1, NL-6525 ED Nijmegen, The Netherlands

E-mail: ses@uet.tu-darmstadt.de

Received 5 May 1999, in final form 19 October 1999

Abstract. We report complementary studies of space-charge distributions in electron-beam irradiated fluoroethylene propylene (FEP) (thicknesses of 13 and 26 μm) using the thermal pulse (TP) method and the laser-induced pressure-pulse (LIPP) method. The distributions obtained by the two methods are compared to show the strengths of both methods, the high near-surface resolution of the TP method (better than 100 nm) and the nearly constant resolution versus depth of the LIPP method (1–2 μm). In addition to the expected implanted negative charge at a depth governed by the electron energy, a negative near-surface charge layer was found close to the metal/FEP interface if the electron beam entered the dielectric through that interface. This finding provides new insights into the charging of dielectrics using electron beams.

1. Introduction

Several acoustic and thermal methods have been developed since around 1980 for measuring charge density, $\rho(z)$, and polarization, $P(z)$, distributions, where z is the thickness coordinate. These methods have been reviewed recently [1]. It is well accepted that the thermal methods have the advantage of a high depth resolution at shallow depths[+] of less than 100 nm, whereas the acoustic methods have the advantage of a good resolution throughout the bulk (1–2 μm). Therefore, both methods can be applied to the same sample to gain complementary information.

In the present paper, we report thermal pulse (TP) [2] and laser-induced pressure-pulse (LIPP) [3] studies of space charge distributions, $\rho(z)$, in electron-beam irradiated fluoroethylene propylene (FEP). This paper is an extension of a prior study [4] comparing $\rho(z)$ obtained by using the thermal wave method (LIMM [5]) and the LIPP method.

The LIMM investigations in [4] disclosed a negative near-surface charge layer (NNSCL) that appeared near the electron-irradiated surface when this surface was metallized. Various NNSCLs have been predicted theoretically [6–8]. These layers arise due to the relaxation of the initially deposited charge in the irradiated region [8]. Relaxation is possible because of the radiation-induced conductivity (RIC) [9]. The negative charges move towards the front surface (where the electron beam entered the sample) in the electric field of the implanted charge.

NNSCLs were also found in LIPP studies near the metallized surface for FEP [3] and the non-metallized side for Mylar™ and Kapton™ films [10]. However, because of the LIPP spatial resolution limitations (1–2 μm) imposed by the pressure-pulse duration (~1 ns), these indications required independent confirmation.

The improvements brought by the present TP measurements [11] compared to the earlier LIMM measurements [4] are extended bandwidth and improved signal-to-noise ratio (SNR) of the measurement. The maximal modulation frequency used for the LIMM spectra in [4] was $f_{max} = 100$ kHz. The time resolution available from the present TP measurements is $t_{min} = 100$ ns (see below), which is equivalent to $f = 1/(2\pi t_{min}) = 1.6$ MHz. Thus,

‖ Permanent address: Kunststoff-Zentrum in Leipzig gGmbH, Erich-Zeigner-Allee 44, D-04229 Leipzig, Germany.
¶ Corresponding author.
[+] For the thermal probing techniques, we understand the term 'depth resolution at shallow depths' as the first grid point of $\rho(z)$ or $P(z)$ inside the sample (with respect to the illuminated side). This 'surface resolution' depends, of course, on the parameters of the equipment employed.

0022-3727/00/040430+07$30.00

compared to the evaluations in [4], the surface resolution (see previous footnote) could be improved by a factor of four. Furthermore, relative to prior LIMM measurements, the SNR was increased by a factor of ∼10, and the number of measuring points, M, was increased by a factor of greater than 2. Consequently, the deconvolution results are expected to be more reliable, especially near the surface.

2. Experimental details

2.1. Samples and charging procedure

The Teflon™ FEP foils were obtained from DuPont de Nemours Deutschland GmbH†. Four samples, identified as A, B, C, and D, were used in the experiments. The thickness of the samples, L, was measured with a mechanical thickness gauge at 10 positions across a sample diameter and mean values (standard uncertainty ∼0.5 μm) were determined to be 13 μm for samples A and B and 26 μm for samples C and D. Before irradiation, an aluminium electrode (∼100 nm thick) was vacuum deposited onto one side of the samples, in our nomenclature the side $z = 0$.

The samples were irradiated with a mono-energetic electron beam [12] by using a modified JEOL JSM-50A scanning electron microscope (see previous footnote) under high vacuum. In all cases, the current density (per side) was 40 μA m^{-2}, the deposited charge (per side) was 1.2 mC m^{-2}, and the energy of the electron beam was $E_b = 25$ keV. Samples A and D were irradiated through the metallized side (at $z = 0$), whereas samples B and C were irradiated through the non-metallized side (at $z = L$). The expected depth of the peak of the electron charge distribution with respect to the surface of electron incidence was 6–7 μm, which was obtained from prior work [13].

After a storage time of about one month in laboratory atmosphere at ∼50% relative humidity (RH), the LIPP measurements were performed. The TP measurements were carried out on the same samples in another laboratory with a delay of about one additional month. For these measurements, an additional metal layer was deposited onto the non-metalized side by an evaporation process.

Differences in sample conditions between the LIPP and the TP experiments are thus (1) additional storage time and (2) deposition of an additional electrode. Both differences do not significantly affect the charge distribution. The effect of the additional storage time can be assessed from surface potential measurements of electron-beam charged FEP [14]. These show that no measureable charge decay occurs over a period of one month, even at a temperature of 70 °C and high humidity. This implies the absence of charge drift in the self-field of the sample and thus the absence of changes in the charge distribution. The effect of a second sample electrode on the charge distribution was investigated in thermal-pulse studies of electron-beam charged FEP films [15]. These experiments yielded very little deviation in mean charge depth of one-side and two-side metalized samples, although there were some slight differences in charging conditions. In addition, a comparison of LIPP results for one-side metalized samples (present study) and for two-side metalized samples [3] indicates no systematic differences in peak depths and shapes. Also, the evaporation process, resulting in a brief heating of the sample to temperatures of 70–80 °C, causes no significant charge drifts in FEP [14].

† Certain commercial materials and equipment are identified in this paper in order to specify adequately the experimental procedure. In no case does such identification imply recommendation or endorsement by the National Institute of Standards and Technology, nor does it imply that the items identified are necessarily the best for the purpose.

2.2. LIPP measurements

The experimental arrangement of the LIPP method for one-side metallized samples has been discussed elsewhere [3, 16]. The measurements were performed with 50 Ω instrumentation and with an air gap (thickness g). Assuming short-circuit conditions, the current from a sample containing only space charge is given by [17]

$$I(t) = \frac{Apt_p}{\rho_m(L + \varepsilon g)}(\gamma + 1)[\rho(z = vt)] \qquad (1)$$

where A, p and $t_p = 70$ ps are the irradiated area, the pressure amplitude, and the pulse duration of the LIPP, respectively. The values ρ_m, ε and v are the mass density, permittivity, and the longitudinal sound velocity of the sample, respectively. The electrostriction constant is given by $\gamma = -\mathrm{d}[\ln(\varepsilon)]/\mathrm{d}S$, where S is the strain [18]. The z coordinate in the sample is related to the time coordinate t according to $z = vt$, where $v = 1.3$ km s^{-1} was used for FEP [3]. In all cases the LIPP was applied to the side at $z = 0$ (the metallized side).

2.3. TP measurements and deconvolution

The TP method has been described in detail elsewhere [2, 11]. The measurements were performed with a modified charge-to-voltage-converter (CVC) (Keithley Instruments) (see previous footnote). Prior to the measurements, the rise time of the CVC was determined with a step generator while the measuring chamber containing the sample was connected to the preamplifier's input. A rise time of ∼30 ns and a settling time of ∼70 ns was obtained.

The TP, measured simultaneously with the TP response by using a fast photodiode, has a Gaussian shape with a width of ∼70 ns. Both the TP and the TP responses were shifted along the time axis so that the time $t = 0$ is at the maximum of the TP. The laser energy was ∼0.1 mJ.

The samples, used before for the LIPP investigations, were each cut into two pieces so as to make the two surfaces ($z = 0$ and $z = L$) available separately as TP-incident surfaces. A second character '0' or 'L' added to the sample designation letter (e.g. A0, AL) denotes the TP incident surface and also identifies the TP responses.

The samples AL, BL, CL, and DL received an additional vacuum-deposited aluminium electrode on the side $z = L$. For samples A0, B0, C0, and D0, the aluminium electrode, which was evaporated on surface $z = 0$ prior to the electron-beam irradiation, and which was not sufficiently thick to absorb most of the energy of the laser pulse, was removed by using a 5% aqueous NaOH solution. All sample surfaces were then carefully cleaned with ultrapure water (resistivity >18 MΩ cm) obtained by using the Milli-Q™ UV Plus system, Millipore Co, Bedford, MA (see previous

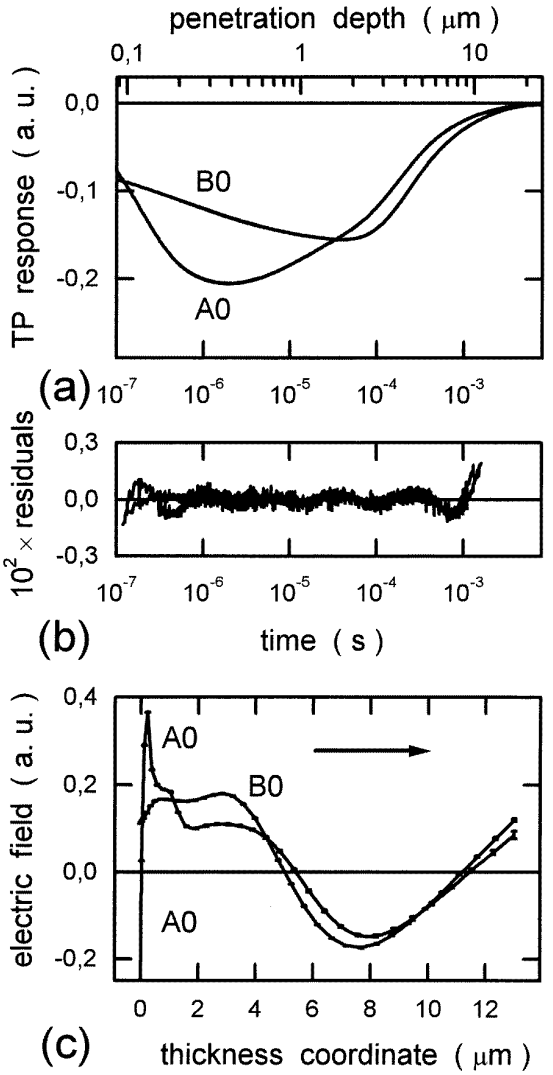

Figure 1. (a) Measured TP response $q(t)$, (b) residuals $d_m(t)$, (c) deconvolved electric field $E(z)$ for samples A0 and B0. The thickness was $L = 13$ μm. TP was applied to $z = 0$. The penetration-depth scale in (a) follows from the time scale according to $\sqrt{(2D_{av}t)}$, where $D_{av} = 3.8 \times 10^{-8}$ m^2 s^{-1}. The arrow in (c) indicates the direction of heat propagation through the samples. a.u. means arbitrary units.

footnote). Afterwards, aluminium electrodes suitable for TP were vacuum deposited on both sides. The thickness of the last deposited electrodes was in all cases 220 nm, as indicated by a Sloan thickness monitor (see previous footnote). Ag-filled epoxy (Duralco^{TM}120, Cotronics Co, Brooklyn, NY) (see previous footnote), was used to glue side $z = L$ of the samples A0, B0, C0, and D0 and side $z = 0$ of the samples AL, BL, CL, and DL to flat copper blocks.

The TP response, $q(t)$, of the sample with electrode area A is a convolution of the electric field, $E(z)$, and the TP-induced temperature increase, $T(t, z)$, as given by the TP equation [18]

$$q(t) = \alpha_C C \int_0^L T(t, z)E(z)\,\mathrm{d}z \qquad (2)$$

where $\alpha_C C = \partial C/\partial T$ is the change of the sample capacity, C, with temperature. The thermal parameters, which are needed to determine the temperature increase $T(t, z)$ by means of the heat conduction equation [4], are the diffusivity, D, and the conductivity, κ, of the sample and the heat transfer coefficient, H_L, between sample and copper block through the glue layer.

The electric-field distribution and the thermal parameters (D, κ, H_L) are determined by a combined deconvolution and variational procedure, consisting of successive deconvolutions, one for each set of thermal parameters. In this procedure, each deconvolution provides a value for the mean square of errors (*MSE*), defined as

$$MSE = \frac{1}{M}\sum_{m=1}^{M} d_m^2 \qquad (3)$$

where the residuals, d_m, are

$$d_m = q(t_m) - q(t_m, E). \qquad (4)$$

The quantity $q(t_m)$ is the measured TP response for the discrete time t_m, and $q(t_m, E)$ is the TP response which is calculated for the deconvolved electric field with the same set of thermal parameters used for the actual deconvolution. By varying (D, κ, H_L) systematically, a global minimum in the minimized *MSE* was found. From this global mimimum, the optimal thermal parameters (D_{opt}, κ_{opt}, $H_{L,opt}$) and the resulting electric field distribution $E(z)$ are obtained. Further details may be found elsewhere [11].

The data analysis range used for all deconvolutions was from $t_{min} = 100$ ns, corresponding to a minimum penetration depth of the heat pulse [19] of $\delta_{min} = \sqrt{(2Dt_{min})} \sim 90$ nm, where $D = 3.8 \times 10^{-8}$ m^2 s^{-1}, to a maximal time, t_{max}, of 2 ms for the samples A and B, and 4 ms for the samples C and D. For samples A and B the number of measuring points was $M \sim 1500$, and for samples C and D this number was $\sim$1700. In the deconvolution, the number of grid points, N, varied between 25 and 35. The statistical error bars for $E(z)$ give a 68% confidence limit.

3. Results

3.1. TP results

In figures 1–4, the TP response, $q(t)$, the residuals, d_m, and the electric field, $E(z)$, are plotted for the samples A, B, C, and D. The relative noise of $q(t)$, as determined in our deconvolution procedure [11], was between 0.2% and 0.3%. The largest d_m values are only slightly greater than the noise amplitude indicating successful deconvolutions. Only in figures 1(b) and 2(b) are there slight deviations of the d_m values from the noise-like behaviour.

The optimal thermal parameters are given in table 1. From the second column in table 1, an averaged diffusivity (with one standard uncertainty), $D_{av} = (3.8 \pm 0.7) \times 10^{-8}$ m^2 s^{-1}, is obtained. The value D_{av} is in agreement with prior results. By using surface temperature measurements [20], Bauer and Ploss found $D = 3.7 \times 10^{-8}$ m^2 s^{-1} for a 12.5 μm thick FEP film, and $D = 5.3 \times 10^{-8}$ m^2 s^{-1} for a 25 μm thick FEP film. In prior LIMM results [4], $D = 5.5 \times 10^{-8}$ m^2 s^{-1} was found. The values for the optimal thermal conductivity are slightly larger than the value

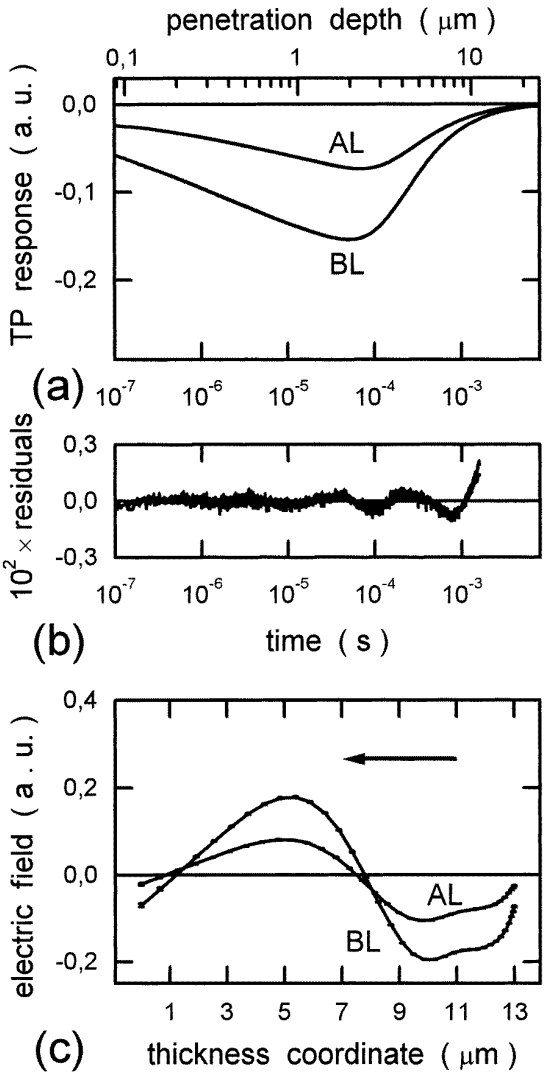

Figure 2. Same as in figure 1, but for AL and BL. The thickness was $L = 13$ μm. TP was applied to $z = L$.

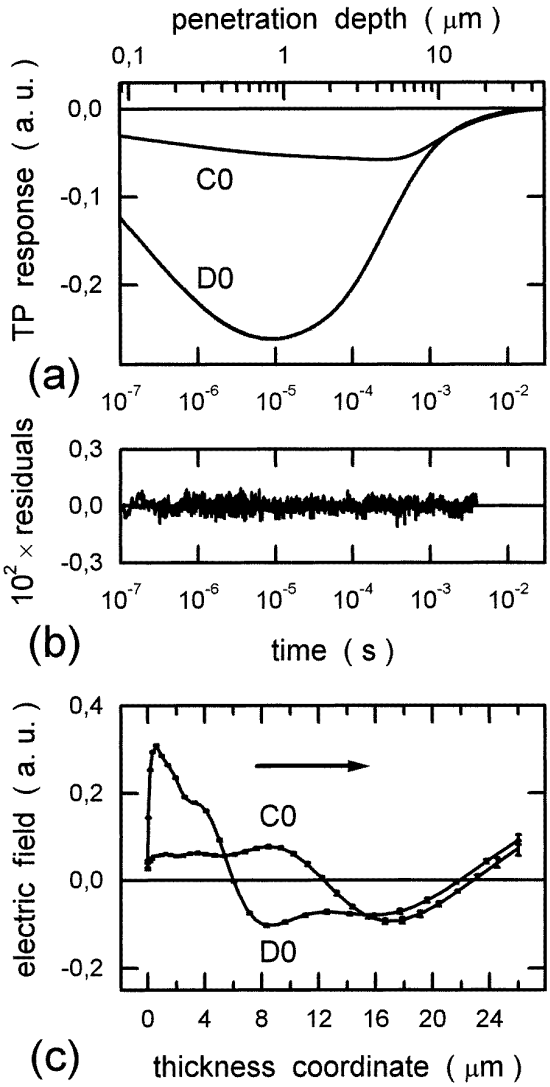

Figure 3. Same as in figure 1, but for C0 and D0. The thickness was $L = 26$ μm. TP was applied to $z = 0$.

Table 1. Values for the optimal thermal parameters determined from the TP responses shown in figures 1–4. The value D_{opt} is the optimal thermal diffusivity, κ_{opt} is the optimal thermal conductivity, and $H_{L,opt}$ is the optimal heat transfer coefficient between the sample and copper block through the glue layer. See text.

Code for response	D_{opt} (10^{-8} m^2 s^{-1})	κ_{opt} (W m^{-1} K^{-1})	$H_{L,opt}$ 10^4 W m^{-2} K^{-1})
A0	4.6	0.28	3.3
AL	3.4	0.24	4.6
B0	3.2	0.22	5.5
BL	3.2	0.22	5.5
C0	3.7	0.23	3.7
CL	4.6	0.20	4.6
D0	4.6	0.26	3.0
DL	3.2	0.23	3.3

0.19 W m^{-1} K^{-1} which can be found in manufacturer data sheets supplied with the samples. From $H_{L,opt}$ the thickness of the glue layers can be determined [11] and was found to vary among samples between 180 μm and 330 μm in agreement with measurement.

3.2. TP charge distributions

In figures 5 and 6, the charge distributions, $\rho(z)$, corresponding to the slope of $E(z)$ are shown by open (for A0, B0, C0, and D0) and full (for AL, BL, CL, and DL) circular symbols connected by thin full curves. The results in figures 5 and 6 have a similar shape to the charge distributions in [4], but the present results are better resolved.

The TP responses of A0 in figure 1(a), D0 in figure 3(a), and CL in figure 4(a) have an extremum at short times, $t_{extr} = (1, \ldots, 12)$ μs, which is equivalent to a peak in $E(z)$ close to the TP side at a heat-penetration depth $\delta_{extr} = \sqrt{(2D_{av}t_{extr})} \sim (0.4, \ldots, 1.0)$ μm (see figures 1(c), 3(c), and 4(c)). From these sharp near-surface peaks in $E(z)$ follow NNSCLs for A0, D0, and CL, as may be seen in figures 5 and 6. Since a peak in the TP responses AL and BL in figure 2(a), B0 in figure 1(a), C0 in figure 3(a), and DL in figure 4(a) appears at longer times ($t_{extr} \geqslant 100$ μs), $E(z)$ has a broad peak or a broad plateau near the TP side. Thus no NNSCL is observed for samples B and C near $z = 0$ and for samples A, B, and D near $z = L$ (figures 5 and 6).

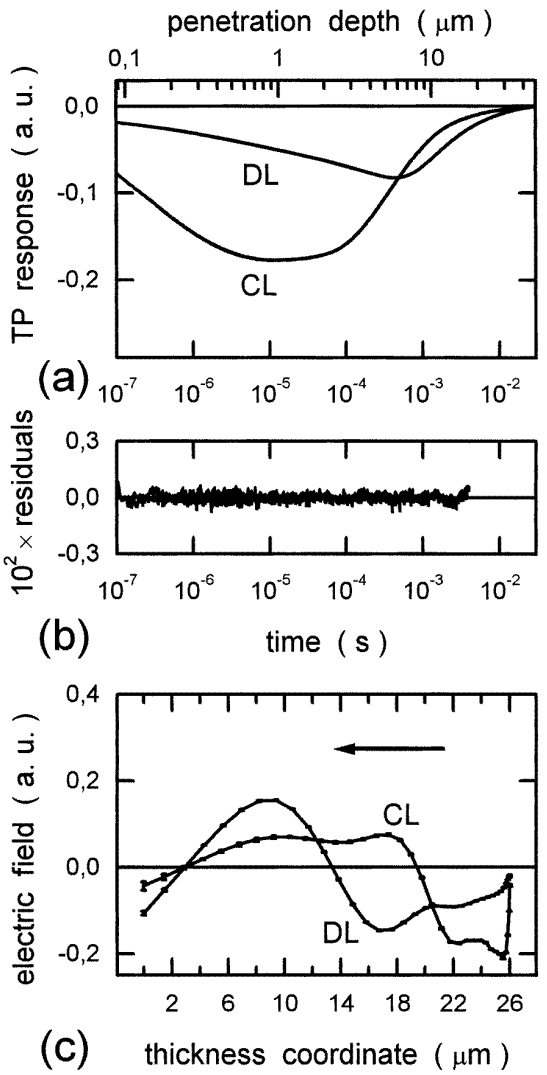

Figure 4. Same as in figure 1, but for CL and DL. Thickness was $L = 26\ \mu$m. TP was applied to $z = L$.

Table 2. The time, t_{extr}, and the corresponding heat-penetration depth, $\delta_{extr} = \sqrt{(2D_{av}t_{extr})}$, where the TP response shows an extremum (part (a) in figures 1–4). For D_{av} the value 3.8×10^{-8} m^2 s^{-1} was used, see text. δ_E is the depth of the peak of the deconvolved electric-field distribution, $E(z)$ (part (c) in figures 1–4). The asterisks indicate samples with field distributions having a broad peak.

Code for response	t_{extr} (μs)	δ_{extr} (μm)	δ_E (μm)
AO	2.0	0.4	0.2
AL(*)	72	2.3	3.1
BO(*)	43	1.8	2.8
BL(*)	52	2.0	3.2
CO(*)	300	4.8	1.2
CL	12	1.0	0.5
DO	9	0.8	0.6
DL(*)	440	5.8	4.0

The depth of the peak of the deconvolved electric field, δ_E, and the values t_{extr} and δ_{extr} are summarized in table 2. A good agreement between δ_{extr} and the corresponding value δ_E can be observed.

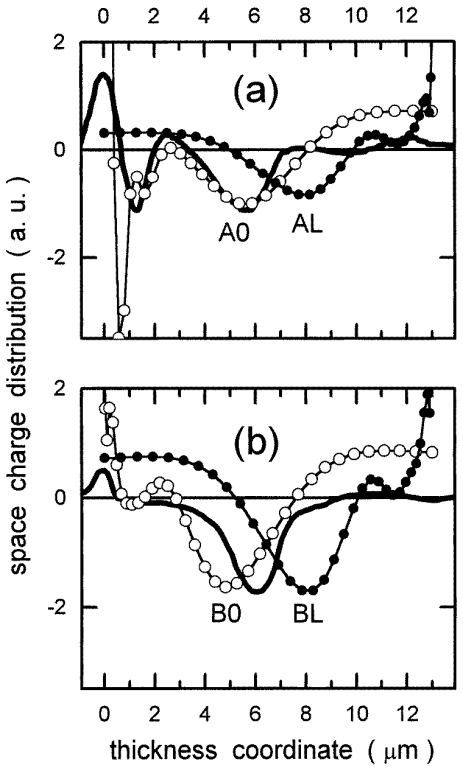

Figure 5. Space charge distributions, $\rho(z)$, for the samples A and B shown in (a) and (b), respectively. Symbols connected with thin full curves are $\rho(z) \propto \mathrm{d}E(z)/\mathrm{d}z$ from the TP method. Open circles indicate the pulsed side at $z = 0$, full circles at $z = L$. The LIPP curves are drawn as thick full curves without symbols. The thickness was $L = 13\ \mu$m.

A positive slope of $E(z)$ near $z = 0$ for A0, B0, C0, and D0, and near $z = L$ for AL, BL, CL, and DL means a positive charge near this side. The value δ_E expresses the depth to which the positive charge extends (of the order of 1 μm). Since the slope of $E(z)$ decreases with z, the peak of the positive charge layer is actually at the surface. This positive charge may be either electrode charge or volume charge in the dielectric material (see also section 3.3).

The charge peaks obtained by primary-electron deposition in the bulk show the following: the peak depths determined by the TP method differ for TP incidence at 0 or L and differ also from the depths obtained by LIPP. The apparent deviations can be explained as follows.

The temperature increases, $T(t, z)$, used for the deconvolution are determined under the assumptions that (i) the influence of the glue layer on $T(t, z)$ can be described by a heat transfer coefficient and that (ii) no temperature increase due to the TP takes place in the substrate. Assumption (i) implies a constant temperature gradient across the glue-layer thickness. This is probably not completely true because of its thickness of being greater than 100 μm. In our simple model, the heat flux from the dielectric into the copper block is overestimated, especially at longer times $t > \tau$. Also, assumption (ii) is not completely valid, even though copper blocks were used as substrates. A local temperature increase in the substrate at the glue/substrate interface would also cause a delay of the heat flux out of the sample.

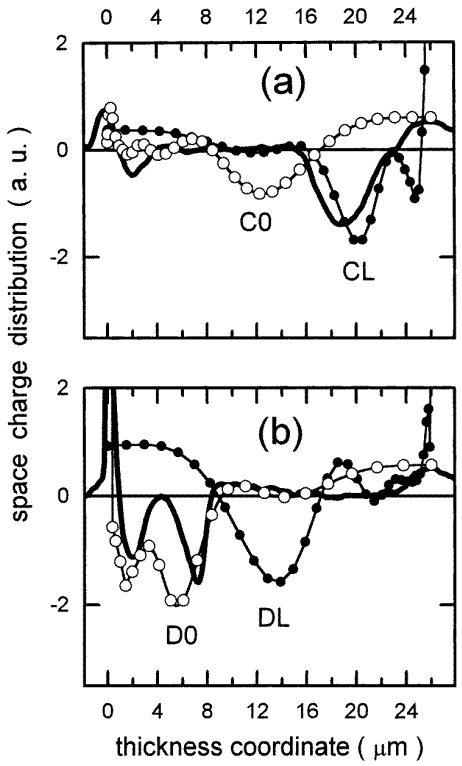

Figure 6. Same as in figure 5, but for samples C and D shown in (a) and (b), respectively. The thickness was $L = 26$ μm.

Because of both assumptions, the $T(t, z)$ values used in the deconvolution are larger than the real ones. Consequently, the so determined field $E(z)$ is smaller than the actual field near the dielectric/substrate interface. This distortion causes a shift of the ρ peak towards the TP side. This hypothesis is supported by the fact that the use of a larger t_{max} in the deconvolution causes a shift of the ρ peak towards the TP side. It should be emphasized that our simulations show an agreement of ρ peaks between assumed and deconvolved $\rho(z)$. Advantageously, in the simulations of the TP responses and the subsequent deconvolutions, the same $T(t, z)$ values are used. Furthermore, it should be kept in mind that the spatial resolution of the thermal methods is $\sim 0.25L$ in the centre of the sample [21] and thus about 3 and 6 μm in the 13 and 26 μm samples, respectively.

3.3. Comparison of charge distributions

In figures 5 and 6 the charge distributions determined by TP (symbols connected with thin curves) and by LIPP (thick full curves) are plotted together for qualitative comparison. The structure of the LIPP responses is reproduced well by the $\rho(z)$ obtained by TP.

The depth of deep-lying LIPP peaks agrees favourably with the expected depth of 6–7 μm (see section 2.1). Deviations of locations of TP and LIPP peaks are less than 2 μm, if one considers only the TP results for the side of the sample which is next to the illuminated surface. The uncertainty of the LIPP depths are estimated to be less than 1 μm assuming a homogeneous pressure wave propagation velocity (no distributed, radiation-induced changes in elastic modulus or density), and neglecting electrical filtering effects in the measuring circuit. Possible reasons for the uncertainty of the TP depths are discussed above. Note that thermal properties are assumed homogeneous (no distributed, radiation-induced changes).

The TP results reflect the expected high resolution on the TP-incident side and the diminished resolution towards the far side. Our simulations show [22] that the charge features near the surface of TP incidence, such as shown in figures 5 and 6, can clearly be resolved by our deconvolution procedure. With increasing distance from the TP-incident side, however, the spatial resolution decreases, see above. Apart from this, similarly electroded and irradiated samples give similar results: AO is similar to DO, BO is similar to CO (high resolution on irradiated side); AL is similar to DL, BL is similar to CL (low resolution because charge features are far from the TP-incident surface).

The NNSCL found from the TP data for A0 and D0 validate the corresponding LIPP peaks, also observed in older data [3]. The depth of these NNSCL is ~ 1 μm, the resolution limit of the LIPP method. Negative charge could come (1) from secondary emission from the metal to the polymer and (2) from charge drift in the irradiated region of the sample. During charging with the electron beam, the beam is partially scattered by the electrode (Al foils are known to scatter electrons) and secondary electrons of lower energy than the primary ones are produced. The range of these secondaries in the sample is very short because of their lower energy and accordingly they are deposited at a shallow depth from the incident surface. In the absence of an electrode on the irradiated surface, these secondaries are not generated and only primary electrons enter the sample. The primary electrons are scattered much less by the polymer than by the electrode and thus produce much fewer secondaries in the sample. Furthermore, the charges can drift due to the finite resistance in the irradiated region promoted by the electric field between the deposited charge and the front-side electrode. It is presently not clear which of the two mechanisms causes the NNSCL.

A weak NNSCL found for CL by TP is not observed by LIPP. This discrepancy may be due to the fact that the TP sample is metallized at $z = L$, resulting in an electric field in the surface region and thus in charge rearrangements. This is not possible in the LIPP sample which is unmetallized at $z = L$.

The positive charge layers extending ~ 1 μm (value δ_E in table 2) from the surface with a peak directly at the surface (see above), found by TP measurements, may be in the dielectric or on the electrode. From LIPP studies, such a layer within the dielectric can only be seen on an unmetallized surface. More studies are needed to identify the positive charge layers seen in the TP data.

4. Conclusions

Space-charge distributions in electron-beam-irradiated FEP (13 and 26 μm thickness) obtained with the LIPP and TP methods were compared. Charge peaks coincide with deviations in location of less than 2 μm, demonstrating the capabilities of the deconvolution algorithm used in this study. Also, negative near-surface charge peaks were detected in

some of the samples. The results show the strengths of the two methods: TP measurements provide large surface resolution while LIPP measurements have good resolution in the volume. Consequently, it is advantageous to apply both methods to the same sample.

Ideally, both measurements are performed on the LIPP equipment, where the short-time data ($t \leqslant L/v$) are representing the LIPP response, while the data at long(er) times ($L/v < t \leqslant L^2/D$) constitute the TP response. By using the LIPP equipment with its short light pulses for obtaining TP data, one can expect even better resolution near the incident surface. Also, such a set-up would be capable of determining charge distributions in non-organic electrets, e.g. silicon dioxide, with thicknesses in the sub-micrometre range.

In order to get better agreement between the charge distributions obtained by deconvolution of TP data and the directly measured LIPP responses, also for deep-lying space-charge peaks, two improvements for the TP method can be suggested for future work. Firstly, the thermal properties of the substrate have to be included in the temperature profile used as integral kernel in the deconvolution. Secondly, the glue layer has to be thinner in order to better fulfil the assumptions for the heat transfer.

Acknowledgments

The TP measurements were performed while PB was a guest researcher at NIST. He is grateful to NIST for the hospitality and for financial support.

References

[1] Sessler G M 1997 *IEEE Trans. Diel. Electr. Insul.* **4** 614–28 and the whole issue of 1996 *IEEE Trans. Diel. Electr. Insul.* **3** (5)

[2] DeReggi A S, Guttman C M, Mopsik F I, Davis G T and Broadhurst M G 1978 *Phys. Rev. Lett.* **40** 413–16

[3] Sessler G M, West J E, Gerhard-Multhaupt R and von Seggern H 1982 *IEEE Trans. Nucl. Sci.* **29** 1644–9

[4] Bloß P, Steffen M, Schäfer H, Yang G-M and Sessler G M 1997 *J. Phys. D: Appl. Phys.* **30** 1668–75

[5] Lang S B and DasGupta D K 1981 *Ferroelectrics* **39** 1249–52

[6] Matsuoka S, Sunaga H, Tanaka R, Hagiwari M and Araki K 1976 *IEEE Trans. Nucl. Sci.* **23** 1447–52

[7] Frederickson A R 1979 Spacecraft charging technology, 1978 *NASA 1979* pp 554–69

[8] Beers B L and Pine V W 1981 Spacecraft charging technology, 1980 *NASA 1981* pp 17–32

[9] Gross B 1987 *Electrets* 2nd edn, ed G M Sessler (Berlin: Springer) section 4.1

[10] West J E, Wintle H J, Berraissoul A and Sessler G M 1989 *IEEE Trans. Electr. Insul.* **24** 533–6

[11] Bloß P, DeReggi A S and Schäfer H *Phys. Rev.* B submitted

[12] Gross B, Gerhard-Multhaupt R, Berraissoul A and Sessler G M 1987 *J. Appl. Phys.* **62** 1429–32

[13] Sessler G M 1989 *IEEE Trans. Electr. Insul.* **24** 395–402

[14] van Turnhout J 1975 *Thermally Stimulated Discharge of Polymer Electrets* (Amsterdam: Elsevier) p 264

[15] von Seggern H, West J E and Kubli R A 1984 *Rev. Sci. Instrum.* **55** 964–7

[16] Sessler G M, West J E and Gerhard R 1982 *Phys. Rev. Lett.* **48** 563–6

[17] Gerhard-Multhaupt R 1983 *Phys. Rev.* B **27** 2494–503

[18] Leal Ferreira G F and Gerhard-Multhaupt R 1990 *Phys. Rev.* B **42** 7317–21

[19] For the equation of the penetration depth, see e.g. Landau L D and Lifschitz E M 1991 *Lehrbuch der Theoretischen Physik* vol VI (Berlin: Akademie) section 51
Poate J M and Mayer J W 1982 *Laser Annealing of Semiconductors* (New York: Academic) p 5

[20] Bauer S and Ploss B 1990 *J. Appl. Phys.* **68** 6361–7

[21] Steffen M, Bloß P and Schäfer H 1996 *Proc. 8th Int. Symp. on Electrets (ISE-8)* (Paris) pp 200–5

[22] Bloß P 1997 Results obtained from extensive simulations performed at NIST 1997, not published